Title: Petrographic carbon in ancient sediments constrains Proterozoic Era atmospheric oxygen levels

Don E. Canfield[1,2,3], Mark A. Van Zuilen[4], Sami Nabhan[4], Christian J. Bjerrum[5], Shuichang Zhang[3], Huajian Wang[3], Xiaomei Wang[3]

Supplementary Information

Raman Spectroscopy

Background

The Raman spectrum of carbonaceous material (CM) in diagenetic and metamorphic rocks has been described in detail (1-4) (5, 6), and a short summary of peak-assignment is given here. The Raman spectrum of CM has a distinct peak at 1580 cm^{-1} (G-peak) representing in-plane E_{2g} bond stretching of carbon in a graphite structure. The presence of defects in the structure causes double resonance effects leading to disorder-related peaks at 1350 cm^{-1} (D1-) and 1620 cm^{-1} (D2-). Strongly disordered organic materials that experienced diagenetic or metamorphic temperatures below ca. 330 ^{o}C also contain out-of-plane defects and dangling bonds causing a broad D3 peak at ~1500 cm^{-1} and shoulders on the D1-peak (most notably a D4-peak at ~1250 cm^{-1}, but in highly disordered materials more peaks can be present). The Proterozoic samples described in this study all have experienced low- to high-grade diagenesis, creating Raman spectra in which, except for a few graphite analyses, the D3- and D4-peaks are present. Recycled carbonaceous materials that experienced metamorphism typically lack the D4-peak (and in most cases also the D3-peak), and they have a prominent narrow G-peak at 1580 cm^{-1} (Figure1, S2). The D1-peak is narrow and small relative to the G-peak, or entirely absent, while the D2 peak is a small, clearly resolved shoulder on the G-peak, or is also entirely absent (Figure 1, S2).

Overall, the entire sequence of organic matter alteration from low-grade diagenesis at 150 ^{o}C to high-grade metamorphism at 640 ^{o}C can be traced by the widths and intensity ratios of these deconvoluted peaks in the Raman spectrum. Since carbonization and graphitization are irreversible, and largely depend on temperature alone (Beyssac et al., 2002), the Raman spectra provide the basis for several Raman spectral peak-based geothermometers. For the relatively low-grade samples used in this study, we applied the geothermometers of (4) and (1), and for the metamorphic recycled components, we used the geothermometer

of (5). Since peak-deconvolution protocols for these geothermometers differ slightly, their specific calculations are discussed below in the section on spectral treatment.

Laser excitation effects during Raman analyses

For this study, two different lasers were used: a 514 nm laser for the initial point analyses and for the hyperspectral maps of samples TZ-21 and WSH-1-2, and a 532 nm laser for random analyses of the other samples. The laser excitation wavelength will affect the positions and relative intensities of the disorder-related peaks in the Raman spectrum (6). The small difference between the two laser wavelengths has therefore caused a systematic spectral discrepancy between the two analytical protocols. The effect of a shift from 514 nm to 532 nm laser has been studied by Aoya et al (6). They found that the resulting differences in the Raman peak characteristics (intensity, FWHM, position) generate an offset in the parameters for geothermometer calculations that is smaller than the typical reported error of geothermometers themselves (ca. 30 to 50 ^{o}C). Therefore, although we note a systematic offset in our initial point analyses and subsequent random point analyses respectively (See supplemental excel file), we do not see critical differences in estimated temperatures as reported in Table 1.

Polishing effects

Polishing of rock thin sections can strongly affect the surface structure of crystalline graphite (7-9). In the upper 10 nm-thick layer of the graphite lattice, double resonance conditions are created that lead to enhanced D1- and D2-peaks in the Raman spectrum. A polished graphite particle can thus appear as a much more disordered carbonaceous material, and this can potentially be mistaken for lower grade metamorphic kerogen. However, the G-peak itself remains unaffected, and only a well-defined D2-peak is generated (7), while peaks D4 and D3 – only found in strongly disordered kerogens – are not observed on polished graphitic surfaces (9). For carbonaceous materials that have experienced greenschist-facies metamorphism or lower, the polishing-

induced effects are much smaller or entirely absent (9). Since all Proterozoic-aged samples used in this study – with the exception of sample SZY-6 – are in the range of diagenesis, recycled fractions of high-grade metamorphic kerogen or graphite could easily be distinguished, regardless of polishing effects.

Table S1. Geochemical and sedimentological characteristics of samples used initial Raman analysis

sample	formation	age Ma	depos envir[a]	type[b]	# analyses	# graphite	TOC wt%	Tmax[c] Lahfid oC	sd	W sum Lahif (°C)	sd	Tmax[d] Kouketsu cm^{-1}	sd	ref
AK-10-53-15	Chuar	742.0	OS/B	C	4	0	20.70	145.7	6.6	190.3	3.2	186.3	2.4	(10)
AK-10-60-32	Chuar	742.0	OS/B	C	2	0	13.70	162.3	13.9	203.3	0.9	184.6	4.1	(11)
SZY-4	Zhengjiaya	1100.0	OS	O	5	0	6.87	309.3	15.0	129.2	4.3	305.5	7.8	(11)
SZY-6	Zhengjiaya	1100.0	OS	O	5	0	9.29	314.9	3.8	134.0	1.9	331.0	6.2	(11)
WSH-1-1	Wenshuihe	1200.0	OS	O	5	0	4.19	283.1	10.5	134.9	7.1	294.5	8.4	(11)
WSH-1-2	Wenshuihe	1200.0	OS	O	5	0	9.29	281.3	21.7	152.3	2.2	285.7	1.5	(11)
TZ-1-7	Taizi	1330.0	OS	O	5	0	5.24	276.0	5.6	136.9	6.2	295.4	10.0	(11)
TZ-21	Taizi	1330.0	OS	O	5	0	4.20	289.7	13.4	144.7	5.4	303.1	11.1	(12)
XML-319-6	Xiamaling Unit 4	1385.0	OS/T	C	12	5	0.06	187.9	7.9	213.6	6.5	202.5	7.0	(13)
XML-362-8	Xiamaling Unit 5	1395.0	OS/T/IF	C	7	0	0.08	191.8	11.2	220.8	7.4	202.1	17.4	(12)
XML-365-45	Xiamaling Unit 5	1395.0	OS/T/IF	C	5	0	0.06	193.1	18.4	206.0	6.4	205.8	10.6	(12)
HSZ-500-6	Hongshuzhuang	1450.0	OS	C	4	0	3.88	172.4	6.9	175.7	2.6	202.5	1.1	Present study
HSZ-511-1	Hongshuzhuang	1450.0	OS	C	3	0	5.94	161.7	10.0	161.0	25.9	202.3	3.2	Present study
HSZ-538-3	Hongshuzhuang	1450.0	OS	C	3	0	2.12	228.1	24.0	156.8	6.8	203.4	2.8	Present study
GYZ-223-6	Gaoyuzhuang	1570.0	OS	C	3	0	2.45	230.3	7.2	145.2	2.9	237.2	6.6	(14)
GYZ-242	Gaoyuzhuang	1570.0	OS	C	5	0	0.08	202.4	4.8	173.2	3.9	233.1	13.1	(14)
GYZ-264-5	Gaoyuzhuang	1570.0	OS	C	3	0	0.82	190.1	16.4	172.8	2.1	235.2	5.8	(14)
GYZ-299-4	Gaoyuzhuang	1570.0	OS	C	5	2	0.15	228.1	24.0	156.8	6.8	235.2	10.2	(14)
MR-2	Reward	1637.0	OS/B	C	3	0	1.37	175.3	13.5	187.3	5.4	218.4	3.4	(15)
MR-4	Reward	1637.0	OS/B	C	4	0	1.40	198.9	3.7	174.4	2.8	227.9	6.5	(15)
MR-8	Reward	1637.0	OS/B	C	3	0	1.80	173.7	8.5	191.3	5.4	215.1	9.8	(15)
MR-9	Reward	1637.0	OS/B	C	7	4	4.40	215.9	6.8	180.1	0.4	222.2	12.6	(15)
MY-2	Wollogorang	1729.0	OS/B	C	4	0	1.37	228.87	5.2	157.8	4.8	258.8	5.1	(15)
MY-7	Wollogorang	1729.0	OS/B	C	3	0	1.90	232.6	3.7	155.0	4.0	259.3	8.0	(15)

[a]OS-outer shelf, B-basin, T-turbidite, IF-iron formation, [b]C-core, O-outcrop, [c]designated T-RA2, [d]defined as sum of peak widths (D1+D2+G), [e]designated T-D1

Table S2. Calculated temperatures from random Raman analyses.

Samples	Formation	age Ma	#[a] temp	Tmax Kouketsu °C	sd	Tmax Lahfid °C	sd	W[c] sum cm^{-1}	sd
AK-10-53-15	Chuar	742.0	43	183.0	15.0	181.2	12.7	224.0	10.8
SZY-6	Zhengjiaya	1100	45	305.0	16.4	321.7[e]	7.6	142.0	13.6
WSH-1-2	Wenshuihe	1200	42	281.8	15.2	280.9	22.4	157.4	8.2
TZ-21	Taizi	1330	57	310.4	13.1	303.3	13.9	142.2	8.0
XML-319-6	Xiamaling Unit 4	1385	49	193.8	12.8	183.7	18.2	224.7	17.7
XML-365-45	Xiamaling Unit 6	1395	10	217.9	14.5	209.0	13.0	209.3	6.5
HSZ-538-3	Hongshuzhuang	1450	54	239.4	7.8	217.6	15.3	202.2	8.6
GYZ-223-6	Gaoyuzhuang	1570	16	257.6	7.8	268.9	17.4	151.2	6.7
GYZ-299-4	Gaoyuzhuang	1570	75	241.1	24.2	253.2	13.8	175.5	14.1
MR-9	Reward	1637	54	238.0	13.9	257.7	13.1	189.1	9.9
MY-2	Wollogorang	1729	80	269.1	9.5	269.6	9.4	165.1	10.0
MY-[e]	Wollogorang	1729	11	251.2	15.2	226.7	6.0	163.8	5.5

[a]number of Raman analysis of sufficient quality for temperature determination

[b]from the Beyssac temperature calibration (5).

[c]sum of peak widths.

Table S3. Minimum oxygen estimates

Samples	Formation	age Ma	max P-1[a]	max P-2[b]	Sediment P-1 Min O_2 0.5 cm y^{-1} %PAL	Sediment P-1 Min O_2 5 cm y^{-1} %PAL	Sediment P-2 Min O_2 0.5 cm y^{-1} %PAL	Sediment P-2 Min O_2 5 cm y^{-1} %PAL	Sediment plus river P-1 Min O_2 0.5 cm y^{-1} %PAL	Sediment plus river P-1 Min O_2 5 cm y^{-1} %PAL	Sediment plus river P-2 Min O_2 0.5 cm y^{-1} %PAL	Sediment plus river P-2 Min O_2 5 cm y^{-1} %PAL
AK10-53-15	Chuar	742	0.552	0.141	0.15	5.36	0.84	15.91	0.09	1.33	0.64	13.00
SZY-6	Zhengjiaya	1100	0.237	0.062	0.55	12.51	1.28	20.49	0.39	9.17	1.12	17.97
WSH-1-2	Wenshuihe	1200	0.230	0.017	0.57	12.74	2.01	25.85	0.41	9.43	1.90	23.70
TZ-21	Taizi	1330	0.0706	0.003	1.21	19.83	3.53	30.66	1.03	17.22	2.17	29.45
XML-319.6	Xiamaling U4	1395	0.003	0.0005	3.65	35.37	3.93	38.56	2.20	30.76	2.22	35.03
HSZ-538.3	Hongshuzhuang	1450	0.047	0.015	1.44	21.48	2.08	26.26	1.34	19.49	1.93	24.16
GYZ-299.4	Gaoyuzhuang	1570	0.003	0.001	3.65	32.38	3.86	36.99	2.18	29.94	2.21	32.15
MR-9	Reward	1637	0.096	0.029	1.05	18.09	1.73	23.40	0.86	15.50	1.66	21.48
MY-2	Wollogorang	1729	0.022	0.009	1.89	24.74	2.68	28.09	1.80	22.61	2.05	26.39

[a]max petrographic carbon from summing max graphite and max kerogen. See Table 1.
[b]max petrographic carbon assuming max kerogen is the same as max graphite.

Table S4. Organic matter distribution

5ths	TOC[a] wt%
1st	0.075
2nd	0.235
3rd	0.612
4th	1.222
5th	2.769

[a]Calculated from Data in (16) omitting data with >4 wt% TOC

Table S5. Average carbon and Sulfur contents of Paleo- and Meso-proterozoic-aged sedimentary rocks

Age Ma	Formation	TOC wt%	S wt%	refs
1729	Wollogorang	3.80	2.00	(15)
1637	Reward	3.94	3.94	(15)
1430	Velkerri lower	0.75	0.23	(17, 18)
1420	Velkarri middle	4.56	0.95	(17, 18)
1410	Velkerri Upper	0.56	0.55	(17, 18)
1405	Xiamaling, U5	0.20	0.18	(12)
1400	Xiamaling, U4	0.13	0.03	(13)
1395	Xiamaling, U3	2.56	0.15	(13)
1390	Xiamaling, U2 lower	3.19	0.52	(13)
1390	Xiamaling, U2 upper	5.56	1.02	(13)
1380	Xiamaling, U1	2.47	1.30	(13)

Table S6. Transport velocities of particle for different river systems calculated by different methods

Basin River	Transport time (kyr)		Length (km)		Transport Velocity (km/yr)		Reference
U-series method	lower	upper	lower	upper	upper	lower	
Himalaya, Ghaghara/Gandak	20	100	800	1000	0.04	0.01	(19) (20)
Mackenzie	9	28	1700	4200	0.47	0.06	(21)
Solimões	4	20	1700	1700	0.43	0.09	(22)
Madeira	14	20	1450	1450	0.10	0.07	(22)
Mean					0.26	0.06	
Geometrical scaling method of Torres et al. (23)							
Bramaputra	2.4		2600		1.11		
Ganges	0.3		2200		8.63		
Mackenzie	4.6		1700		0.37		
Amazon	7.4		6400		0.86		
Solimões	13.2		1700		0.13		
Madeira	0.2		1450		7.67		
Mean:	4.7				3.13		
Model fit to observed Kerogen oxidation:	17.9		6000		0.34		

Figure S1a

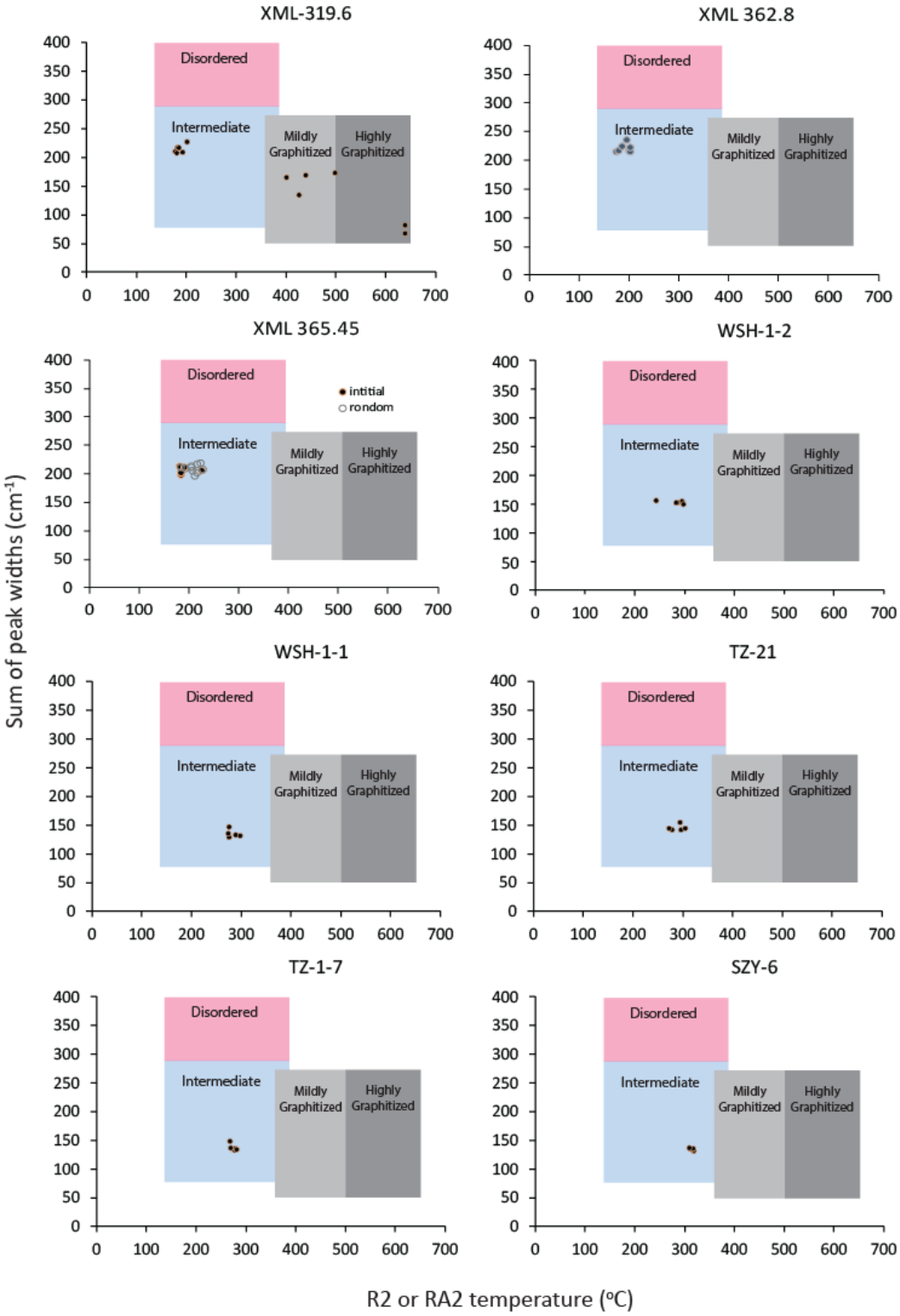
XML-319.6
XML 362.8
XML 365.45
WSH-1-2
WSH-1-1
TZ-21
TZ-1-7
SZY-6
Disordered
Intermediate
Mildly Graphitized
Highly Graphitized
intitial
rondom
Sum of peak widths (cm-1)
R2 or RA2 temperature (°C)

Figure S1b

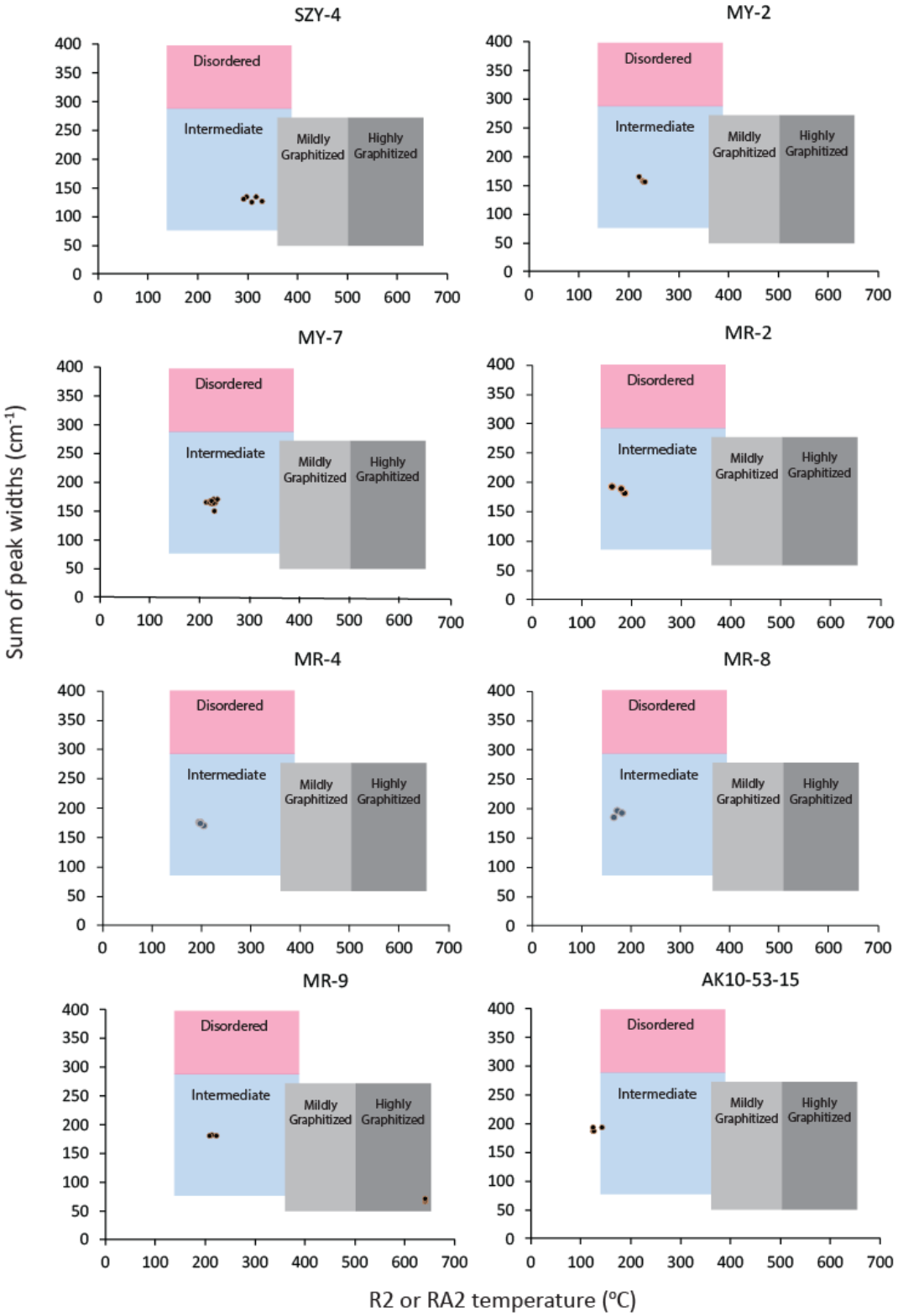
SZY-4
MY-2
MY-7
MR-2
MR-4
MR-8
MR-9
AK10-53-15
Disordered
Intermediate
Mildly Graphitized
Highly Graphitized
Sum of peak widths (cm-1)
R2 or RA2 temperature (°C)

Figure S1c

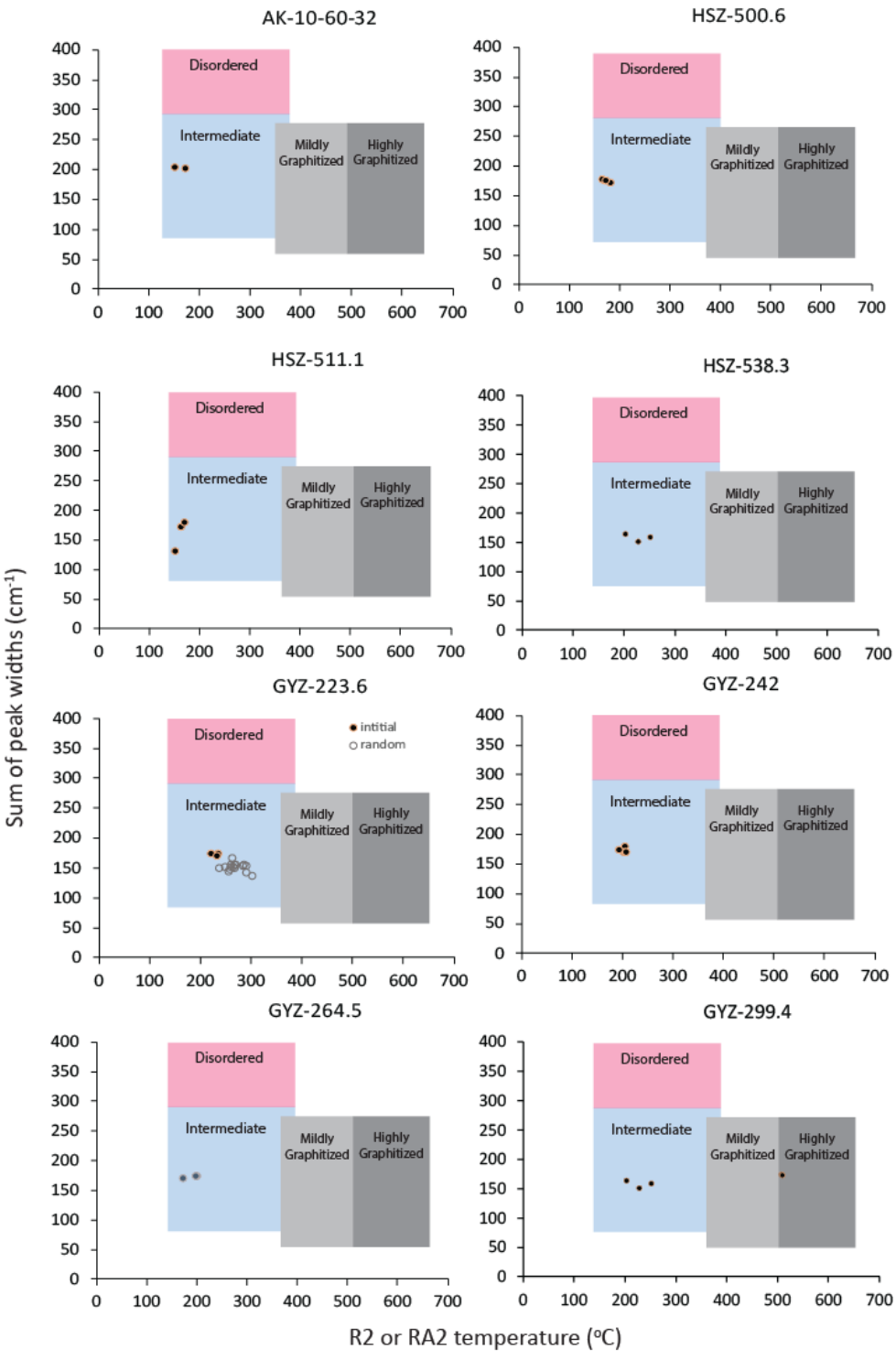

Figure S1. Initial Raman results from a number of different samples covering a total of 9 different geologic formations of Proterozoic age. The dated plotted on a "Sparkes" plot. Also shown are different regions of thermal maturity. Samples from XML 365.45 and GYZ 223.6 also contain a limited data set of "random" Raman analyses. Further information on the numbers of data points and the depositional settings of these samples are found in Table S1.

Figure S2

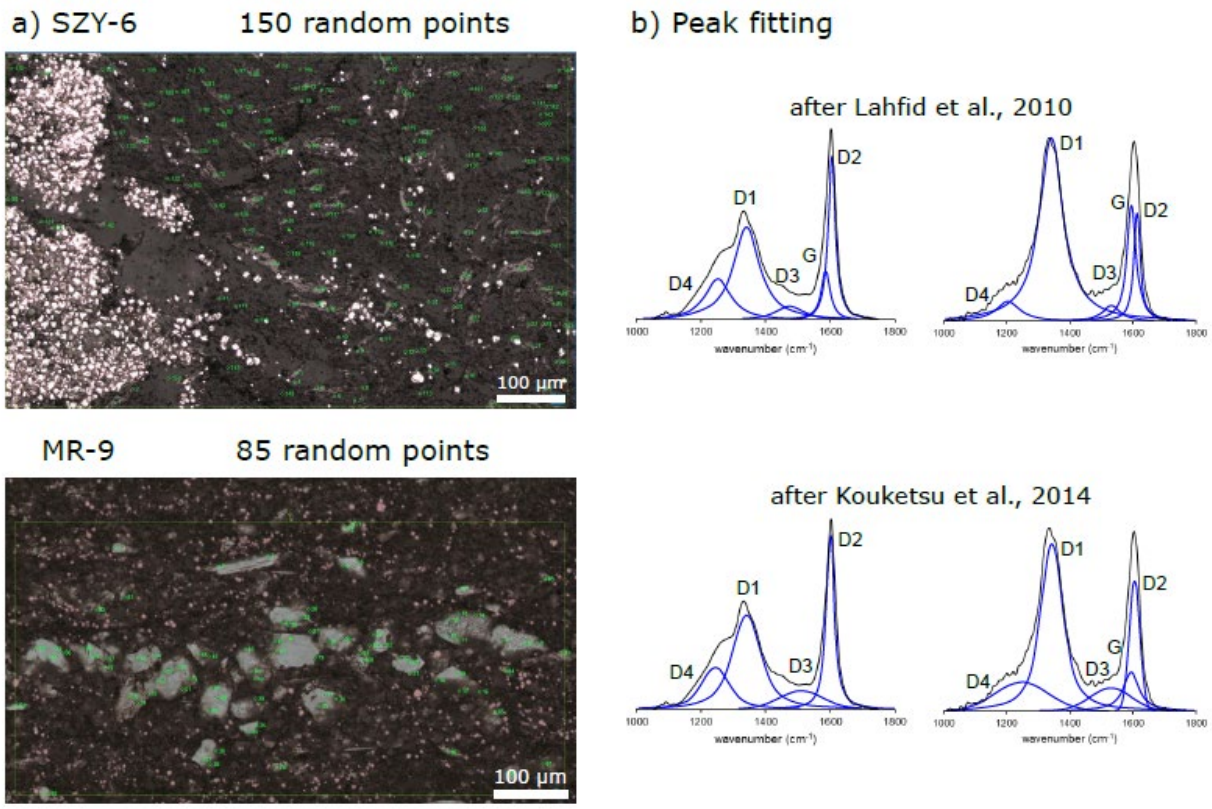

Figure S2. Panels on left show the distribution of random points for samples SZY-6 and MR-9. The panels on the right show curve fitting details for both the Lahfid and Kouketsu geothermometers.

Figure S3

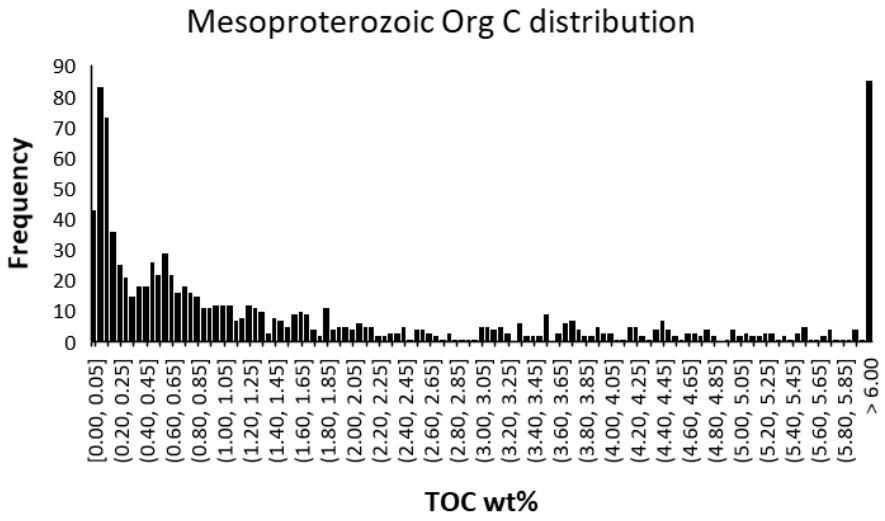

Figure S3. Frequency distribution of TOC concentrations from Mesoproterozoic and latest Paleoproterozoic sedimentary rocks. Data from (16).

Figure S4

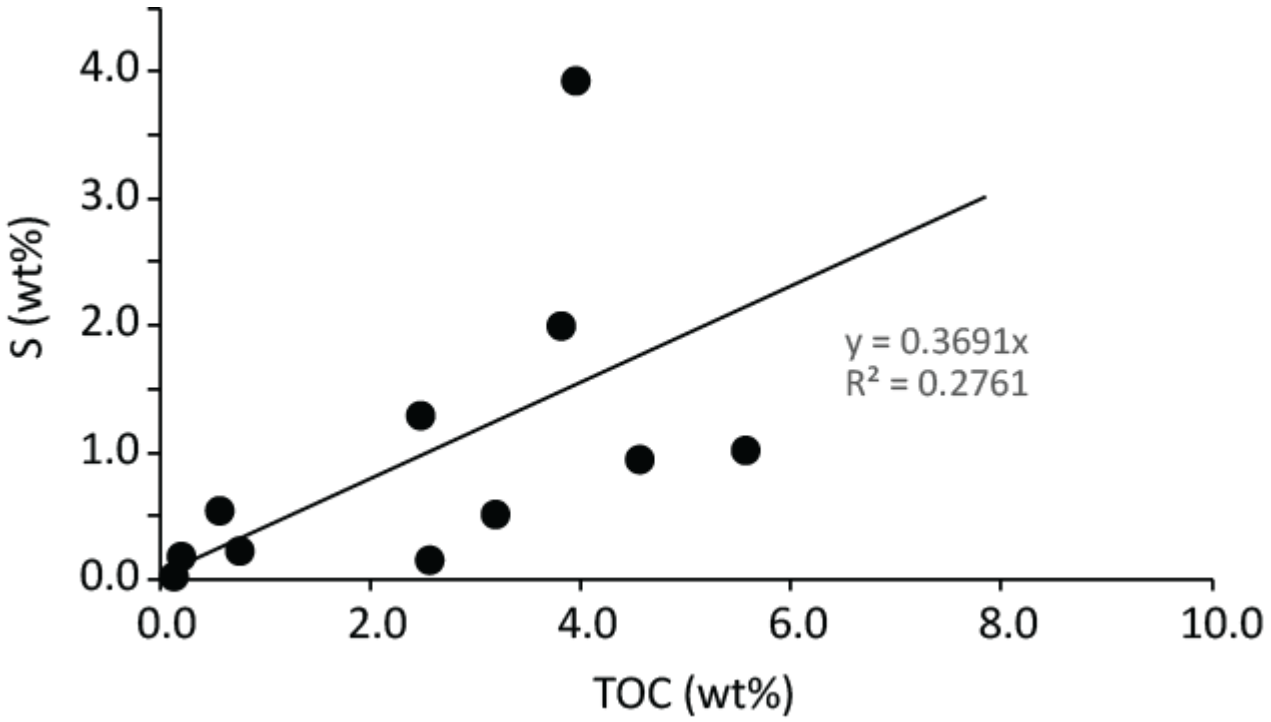

Figure S4. Formation average organic carbon versus sulfur for Mesoproterozoic sedimentary rocks. See Table S5 for data.

Fig S5

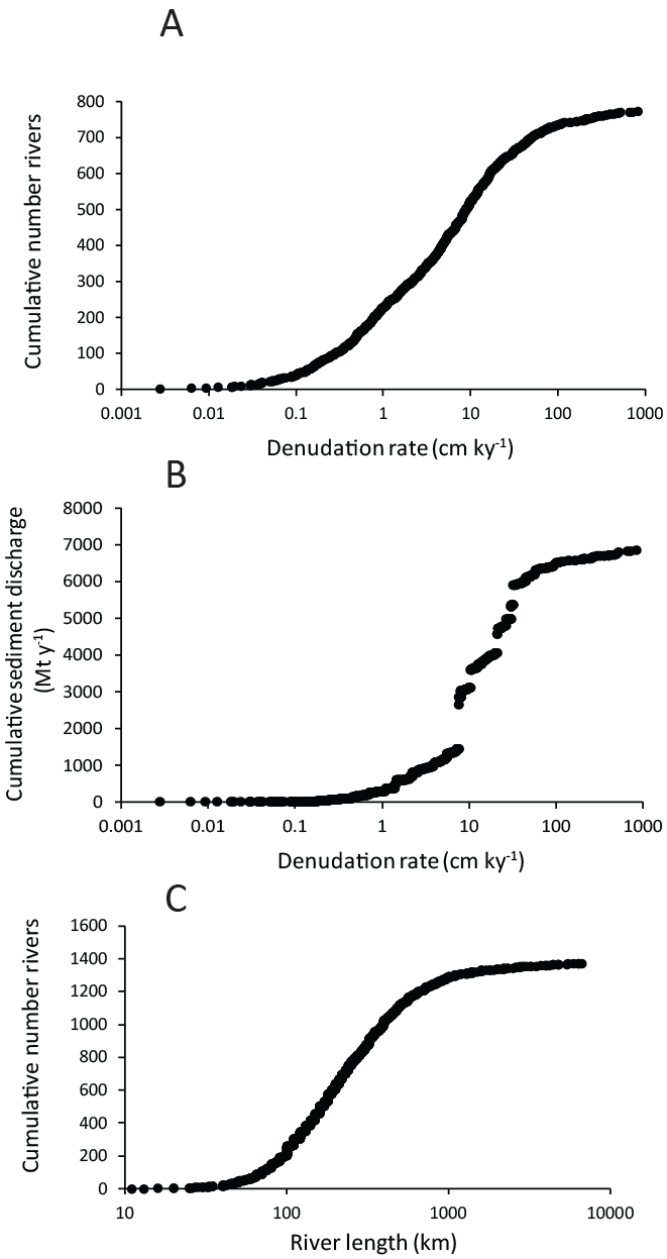

Figure S5. A) cumulative number of rivers as a function of denudation rate, B) cumulative sediment discharge as a function of denudation rate, C) cumulative number of rivers as a function of river length. Data from (24). Note that only a fraction of the rivers listed in the exhaustive database of (24) have suspended sediment data, so the total sediment discharge represented in B) is less than the estimated sediment discharge to the oceans of of 19,000 Mt y^{-1} (24). We assume, however, that the pattern of cumulative sediment discharge as a function of denudation rate as shown in B) reflects the pattern in general.

Figure S6

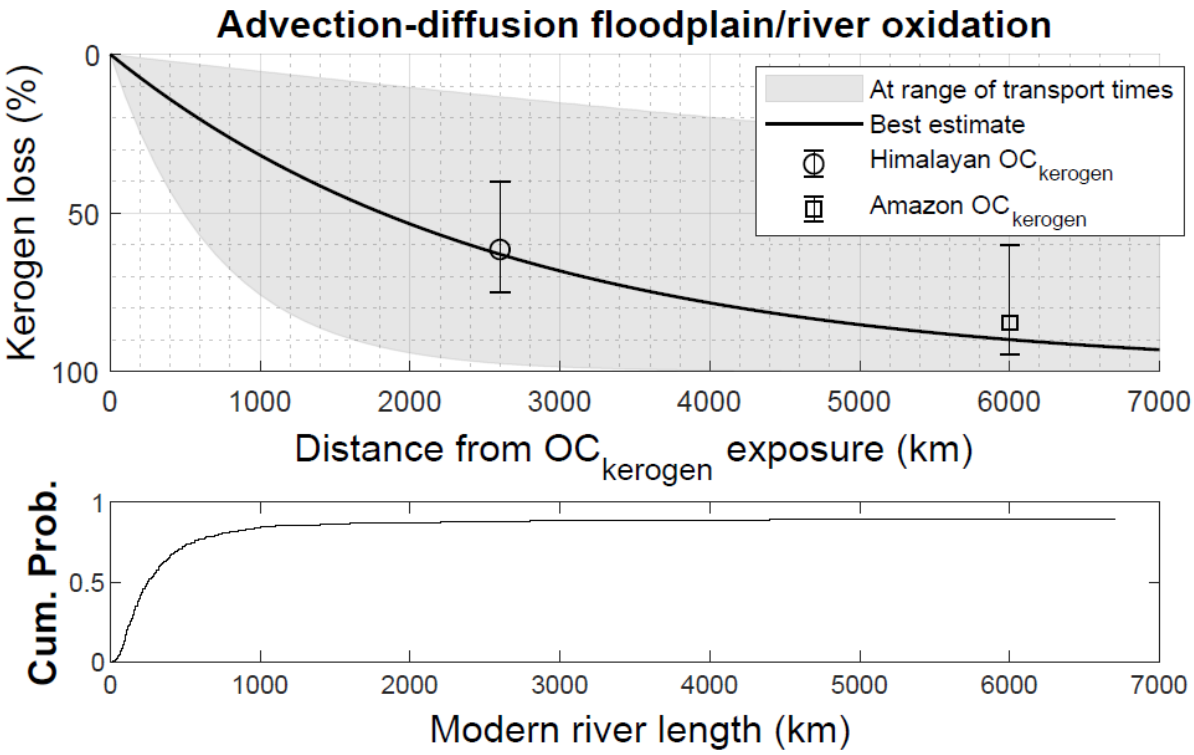

Figure S6. Petrographic kerogen carbon mass loss through oxidation during river and floodplain transport as modelled with a reaction-transport-diffusion model. Gray envelope is based on range of effective transport times reported in the literature. In our model, we choose an effective transport time that reproduces both the observations of petrographic kerogen carbon mass loss for the Ganges-Brahmaputra river system and the Amazon system. The bottom graph shows the cumulative probability of modern river lengths with data from ref (24). See Supplemental text for details

Figure S7.

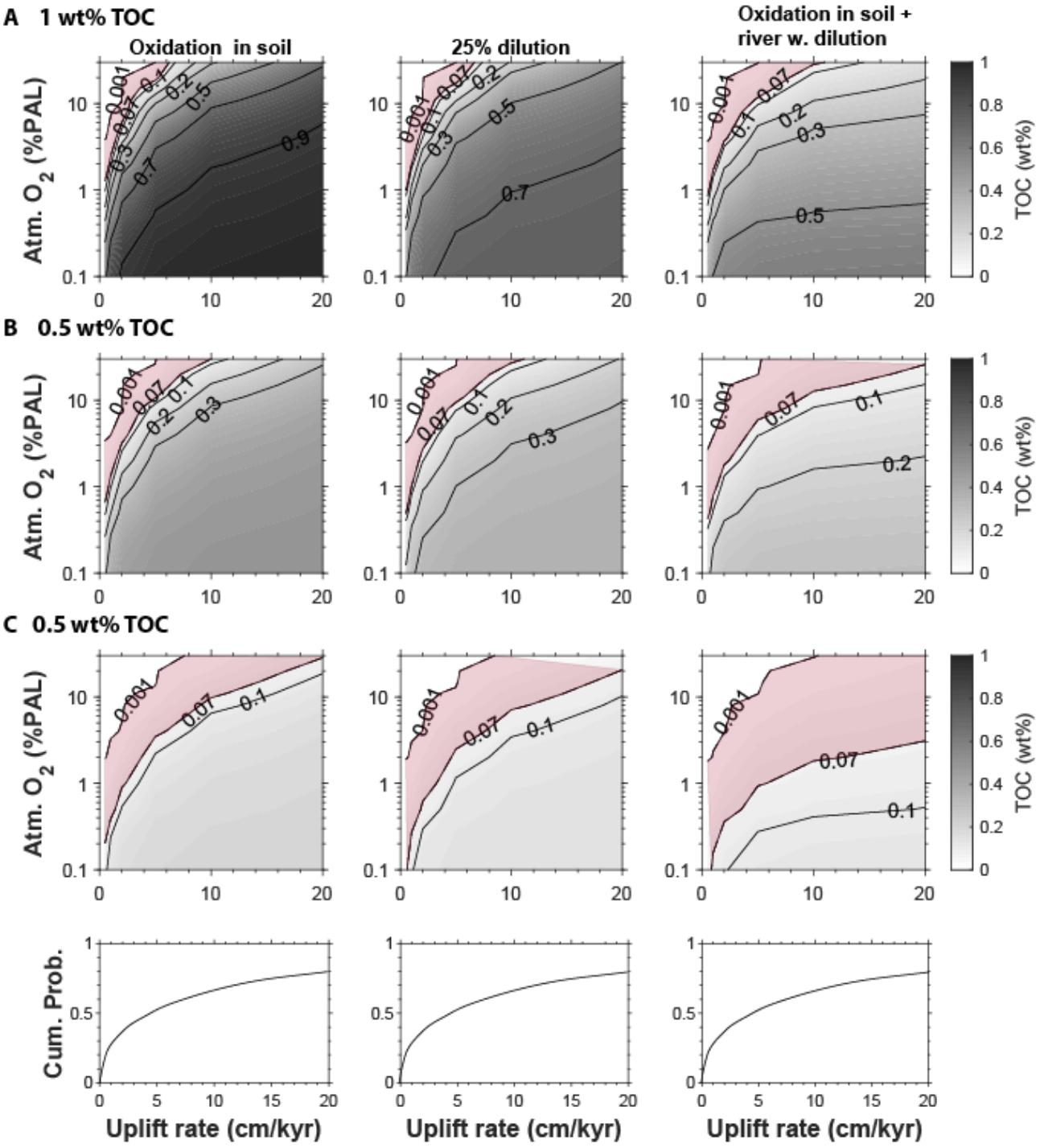

Figure S7. Sensitivity analysis for carbon oxidation model with three different concentrations of TOC in the weathering soil. A) 1 wt% TOC, B) 0.5 wt% TOC and C) 0.2 wt% TOC. These results contrast with those in the main text where a distribution of different TOC concentrations was integrated to yield the final model results. The left panel shows the concentrations of organic carbon

expected in the surface soils. The middle panel shows the concentrations of petrographic carbon exported to marine sediments accounting for dilution by the weathering of clastic particles from non-sedimentary rocks. The panel on the right shows the concentrations of petrographic carbon exported to marine sediments including also oxidation during river transport. The blue field shows the likely range of uplift for the terrains supplying particles to the sedimentary rocks of our study. The bottom graphs show the cumulative probability of uplift rate for modern river basins assuming that denudation rate and uplift rate can be equated.

SI references

1. A. Lahfid *et al.*, Evolution of the Raman spectrum of carbonaceous material in low-grade metasediments of the Glarus Alps (Switzerland). *Terra nova* **22**, 354-360 (2010).
2. M.-C. Sforna, M. Van Zuilen, P. Philippot, Structural characterization by Raman hyperspectral mapping of organic carbon in the 3.46 billion-year-old Apex chert, Western Australia. *Geochimica et Cosmochimica Acta* **124**, 18-33 (2014).
3. F. Delarue *et al.*, The Raman-derived carbonization continuum: A tool to select the best preserved molecular structures in Archean kerogens. *Astrobiology* **16**, 407-417 (2016).
4. Y. Kouketsu *et al.*, A new approach to develop the R aman carbonaceous material geothermometer for low-grade metamorphism using peak width. *Island Arc* **23**, 33-50 (2014).
5. O. Beyssac, B. Goffé, C. Chopin, J. Rouzaud, Raman spectra of carbonaceous material in metasediments: a new geothermometer. *Journal of metamorphic Geology* **20**, 859-871 (2002).
6. M. Aoya *et al.*, Extending the applicability of the Raman carbonaceous-material geothermometer using data from contact metamorphic rocks. *Journal of Metamorphic Geology* **28**, 895-914 (2010).
7. M. Ammar, J. N. Rouzaud, How to obtain a reliable structural characterization of polished graphitized carbons by Raman microspectroscopy. *Journal of Raman spectroscopy* **43**, 207-211 (2012).
8. O. Maslova, M. Ammar, G. Guimbretière, J.-N. Rouzaud, P. Simon, Determination of crystallite size in polished graphitized carbon by Raman spectroscopy. *Physical Review B* **86**, 134205 (2012).
9. Y. Qu, M. A. van Zuilen, A. Lepland, Hydrothermal circulation and oil migration at the root of the heterogeneous micro-structure of carbonaceous material in the 2.0 Ga Zaonega Formation, Onega Basin, Russia. *Precambrian Research*, 105705 (2020).
10. T. W. Dahl *et al.*, Molybdenum evidence for expansive sulfidic water masses in ~750 Ma oceans. *Earth and Planetary Science Letters* (2011).
11. D. E. Canfield *et al.*, Highly fractionated chromium isotopes in Mesoproterozoic-aged shales and atmospheric oxygen. *Nature communications* **9**, 2871 (2018).
12. D. E. Canfield *et al.*, A Mesoproterozoic iron formation. *Proceedings of the National Academy of Sciences* 10.1073/pnas.1720529115 (2018).
13. X. Wang *et al.*, Oxygen, climate and the chemical evolution of a 1400 million year old tropical marine setting. *American Journal of Science* **317**, 861-900 (2017).
14. S. Zhu *et al.*, Decimetre-scale multicellular eukaryotes from the 1.56-billion-year-old Gaoyuzhuang Formation in North China. *Nature Communications* **7** (2016).
15. Y. Shen, D. E. Canfield, A. H. Knoll, Middle Proterozoic ocean chemistry: Evidence from the McArthur Basin, Northern Australia. *American Journal of Science* **302**, 81-109 (2002).
16. D. E. Canfield, C. J. Bjerrum, S. Zhang, H. Wang, X. Wang, The modern phosphorus cycle informs interpretations of Mesoproterozoic Era phosphorus dynamics. *Earth-Science Reviews*, 103267 (2020).

17. G. M. Cox *et al.*, Basin redox and primary productivity within the Mesoproterozoic Roper Seaway. *Chemical Geology* **440**, 101-114 (2016).
18. K. Nguyen (2014) A Geochemical Study of the 1.4 Ga Roper Group, Northern Australia: A Window to Environmental Conditions and Life During the Mid-Proterozoic. in *Geology* (UC Riverside, Riverside, California), p 45.
19. M. Granet, F. Chabaux, P. Stille, C. France-Lanord, E. Pelt, Time-scales of sedimentary transfer and weathering processes from U-series nuclides: clues from the Himalayan rivers. *Earth and Planetary Science Letters* **261**, 389-406 (2007).
20. M. Granet *et al.*, U-series disequilibria in suspended river sediments and implication for sediment transfer time in alluvial plains: the case of the Himalayan rivers. *Geochimica et Cosmochimica Acta* **74**, 2851-2865 (2010).
21. N. Vigier, B. Bourdon, S. Turner, C. J. Allègre, Erosion timescales derived from U-decay series measurements in rivers. *Earth and Planetary Science Letters* **193**, 549-563 (2001).
22. A. Dosseto, B. Bourdon, J. Gaillardet, C. Allègre, N. Filizola, Time scale and conditions of weathering under tropical climate: Study of the Amazon basin with U-series. *Geochimica et Cosmochimica Acta* **70**, 71-89 (2006).
23. M. A. Torres *et al.*, Model predictions of long-lived storage of organic carbon in river deposits. *Earth Surface Dynamics* **5**, 711-730 (2017).
24. J. D. Milliman, K. L. Farnsworth, *River discharge to the coastal ocean: a global synthesis* (Cambridge University Press, 2013).